*Supplementary Information*

# 4D printed nanoengineered super bioactive hydrogel scaffold with programmable deformation for potential bifurcated vascular channel construction

*Amit Nain,[a,]* Akshat Joshi,[b] Souvik Debnath,[a] Saswat Chodhury,[c] Jobin Thomas,[d] Jitendra Satija,[d] Chih-Ching Huang,[e,f] Kaushik Chatterjee[a,c,]**

[a]*Department of Material Engineering, Indian Institute of Science, Bangalore, Karnataka 560012, India*
[b]*Terasaki Institute for Biomedical Innovation, Los Angeles, CA 90024, USA*
[c]*Department of Bioengineering, Indian Institute of Science, Bangalore, Karnataka 560012, India*
[d]*Centre for Nanobiotechnology, Vellore Institute of Technology, Vellore, Tamil Nadu 632014, India*
[e]*Department of Bioscience and Biotechnology and Centre of Excellence for the Oceans, National Taiwan Ocean University, Keelung, 202301, Taiwan*
[f]*School of Pharmacy, College of Pharmacy, Kaohsiung Medical University, Kaohsiung, 80708, Taiwan*

**Corresponding author (s): amitnain@iisc.a.cin (A.N.) & kchatterjee@iisc.ac.in (K.C.)*

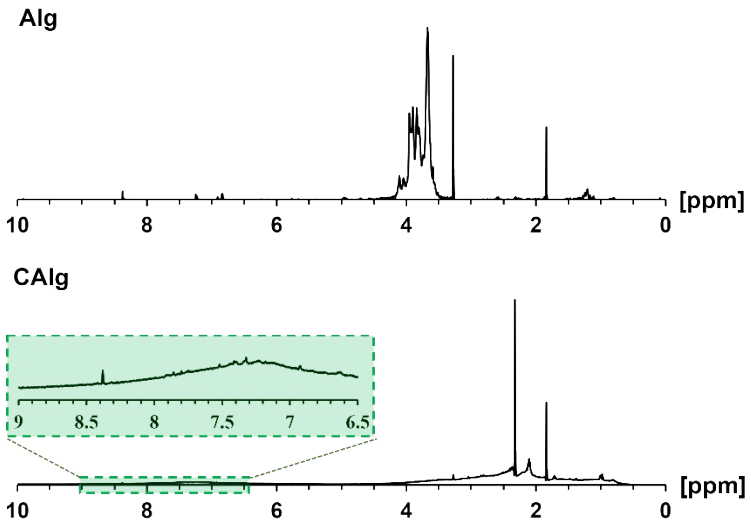


**Fig. S1.** The $^{1}$H-NMR spectra of Alg and CAlg at a concentration of 50 mg mL$^{-1}$ in $D_2O$ at 298 K. Inset in CAlg is the spectra from 6.5–9.0 ppm.

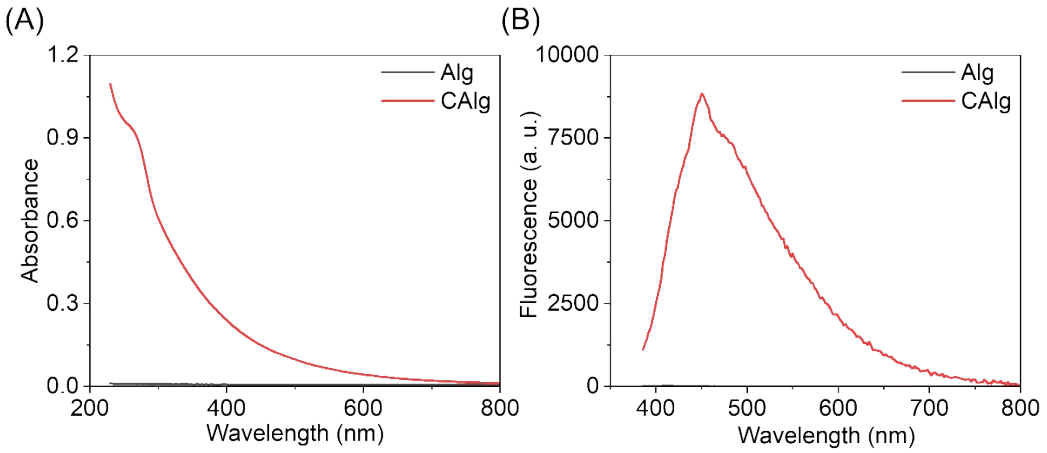


**Fig. S2:** (A) UV-visible absorption and (B) photoluminescence spectra of alginate before (Alg) and after (CAlg) heating.

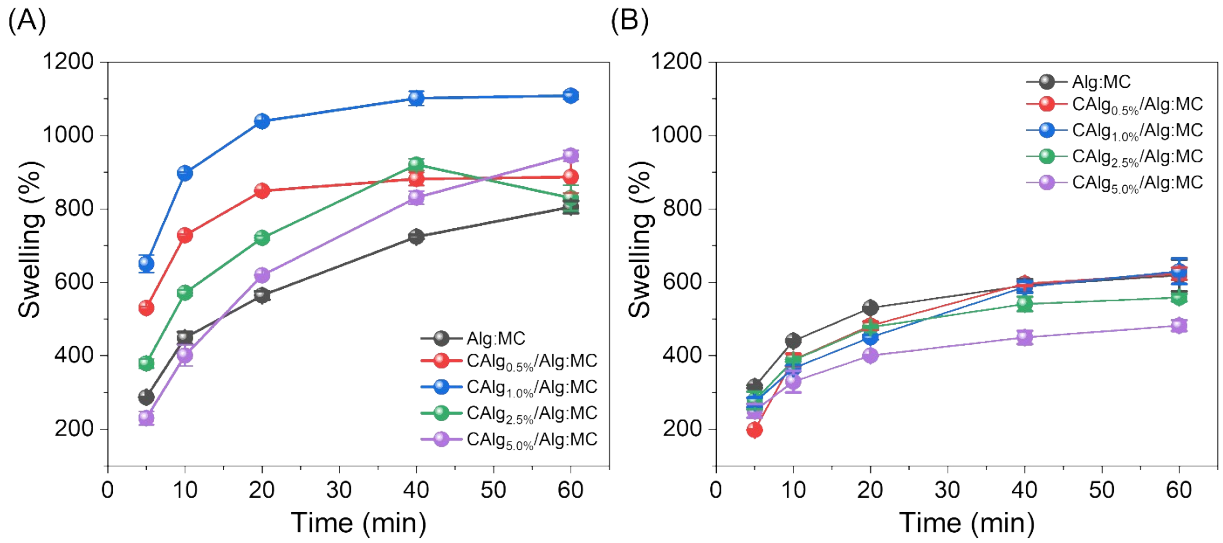


**Fig. S3:** Swelling behavior of CAlg/Alg:MC hydrogel (CAlg=0-5wt.%) prepared using (A) 3:9 and (B) 4:6 composition in DI water.

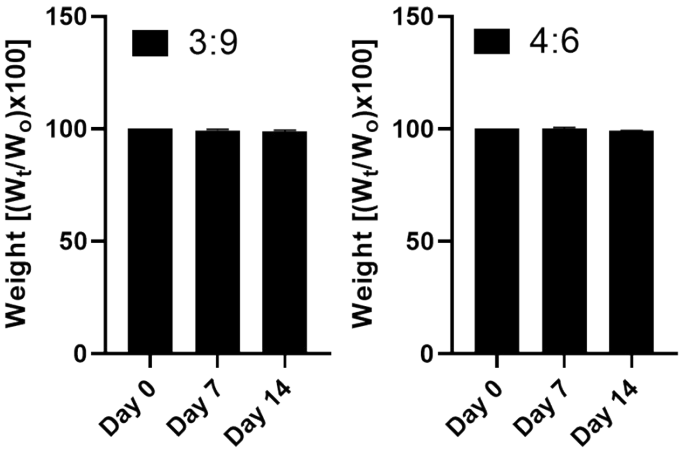


**Fig. S4:** Degradation behavior of CAlg/Alg:MC hydrogels (CAlg=2.5wt.%) in phosphate-buffered saline.

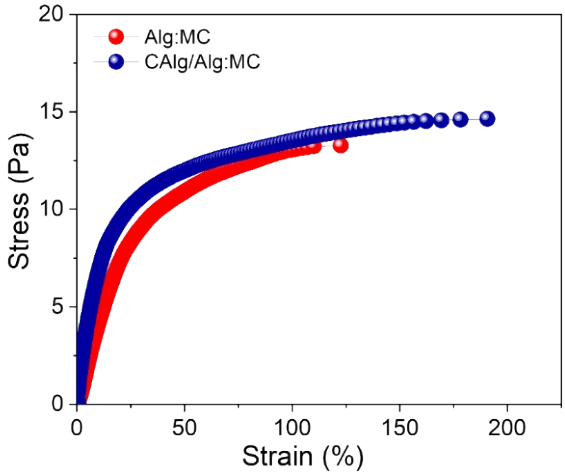


**Fig. S5:** Stress-strain curve of pristine Alg:MC and nanoengineered CAlg/Alg:MC hydrogel under uniaxial tensile force at a force rate of 0.1 N $mm^{-1}$.

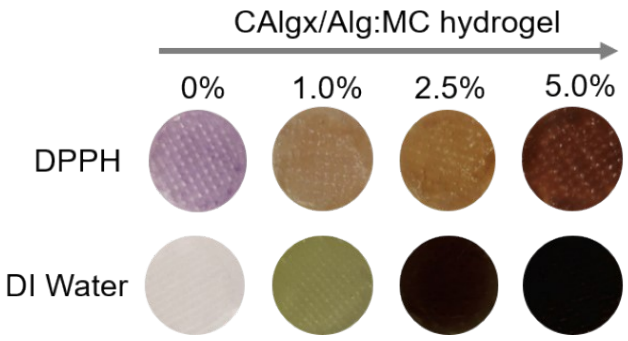


**Fig. S6:** Disc-shaped (diameter 10 mm and thickness 0.25 mm) 3D-printed CAlg/Alg:MC hydrogel (CAlg=0-5wt.%) immersed in 2,2-diphenyl-1-picryl-hydrazyl-hydrate (DPPH) solution for 1 h. Other conditions are the same as in Figure 3B.

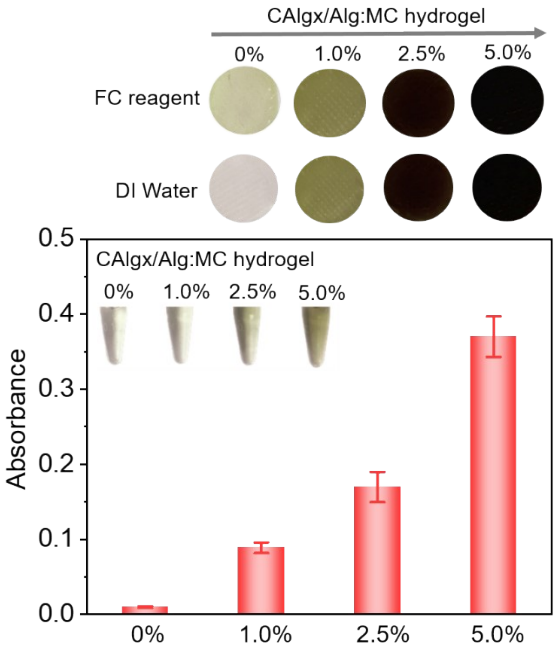


**Fig. S7:** The absorbance of Folin-Ciocâlteu (FC) reagent (0.0125 N) at 765 nm incubated with CAlg/Alg:MC (CAlg=0-5wt.%) for 1 h, in the presence of $Na_2CO_3$ (0.1 M). Data are presented as mean ± SD (n = 3).

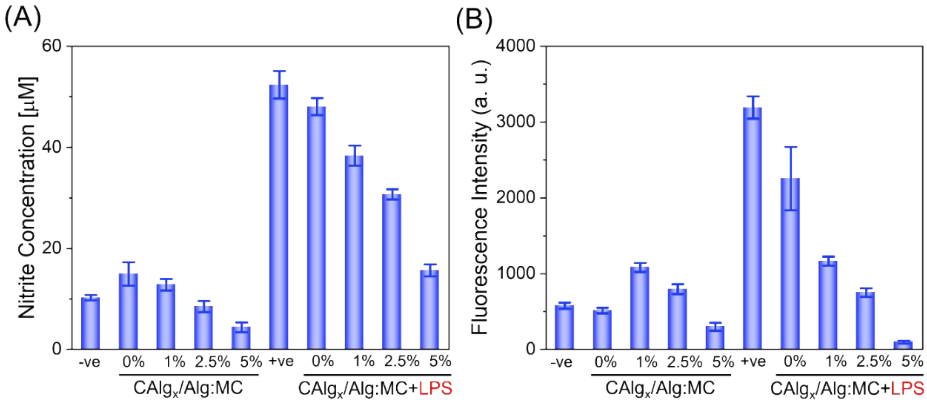


**Fig. S8:** Estimation of (A) nitrite (absorbance at 540 nm) and (B) DCF fluorescence intensity (excitation/emission wavelength; 490/530 nm) in RAW264.7 macrophages incubated in the absence and presence of CAlg/Alg:MC (CAlg=0-5wt.%) in 5% $CO_2$ at 37 °C for 24 h using Griese reagent and DCFH-DA assay, respectively. Data are presented as mean ± SD (n = 3).

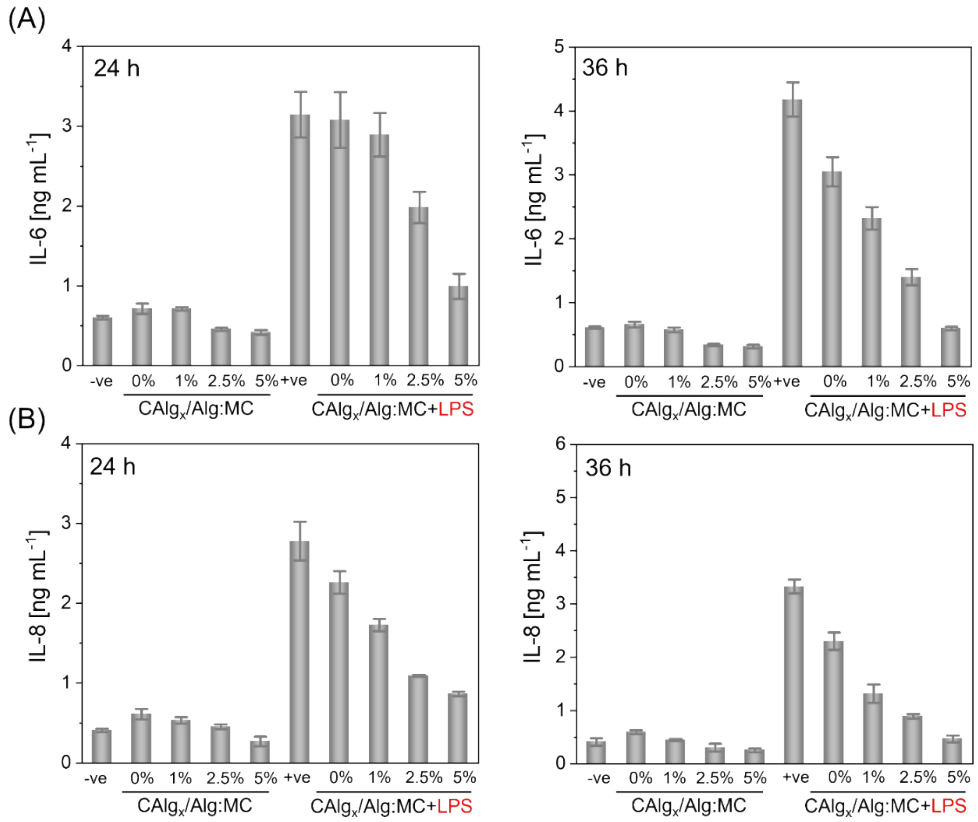


**Fig. S9:** Concentrations of pro-inflammatory cytokines (IL-6 and IL-8) in the RAW264.7 macrophages incubated in the absence and presence of CAlg/Alg:MC (CAlg=0-5wt.%) in 5% $CO_2$ at 37 °C for 24 h and 36 h were determined using ELISA. Data are presented as mean ± SD (n = 3).

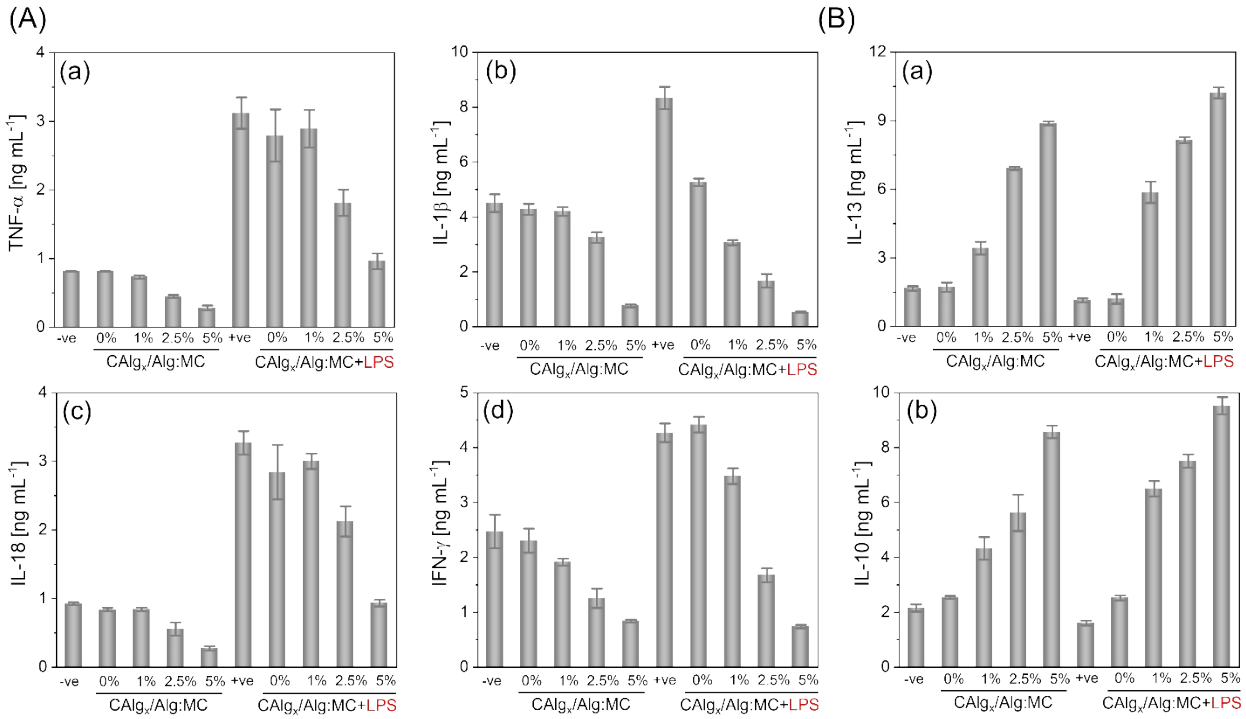


**Fig. S10:** Concentrations of (A) pro-inflammatory cytokines, (A-a) TNF-α, (A-b) IL-1β, (A-c) IL-18, and (A-d) IFN-γ and (E) anti-inflammatory cytokines, (B-a) IL-13 and (B-b) IL-10 in the RAW264.7 macrophages incubated in the absence and presence of CAlg/Alg:MC (CAlg=0-5wt.%) in 5% $CO_2$ at 37 °C for 24 h were determined using ELISA. Data are presented as mean ± SD (n = 3).

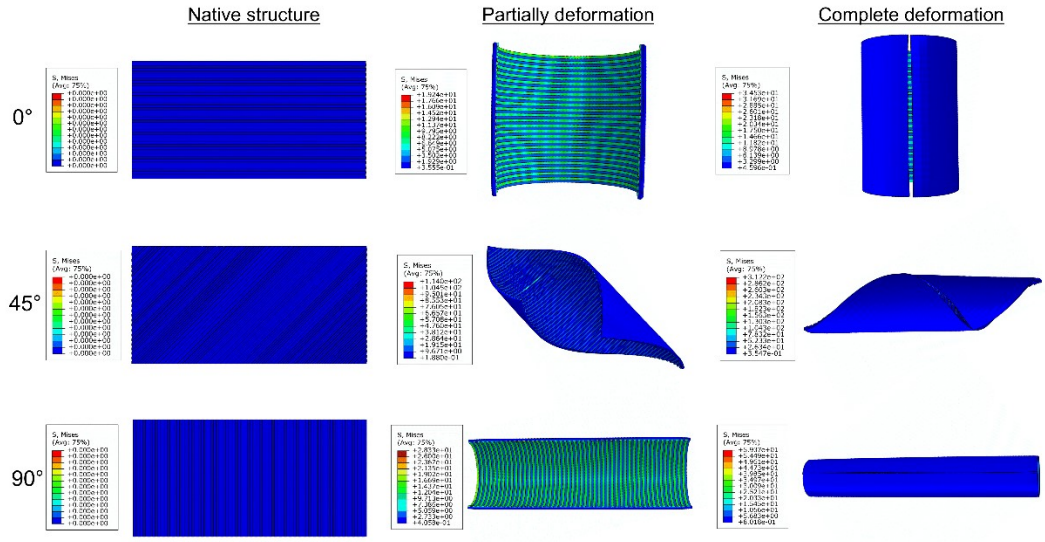


**Fig. S11:** FEA simulations of tubular geometries showing different stripe angles and subsequent effects of stripe angle (0º, 45º and 90º) on corresponding deformations determined computationally.

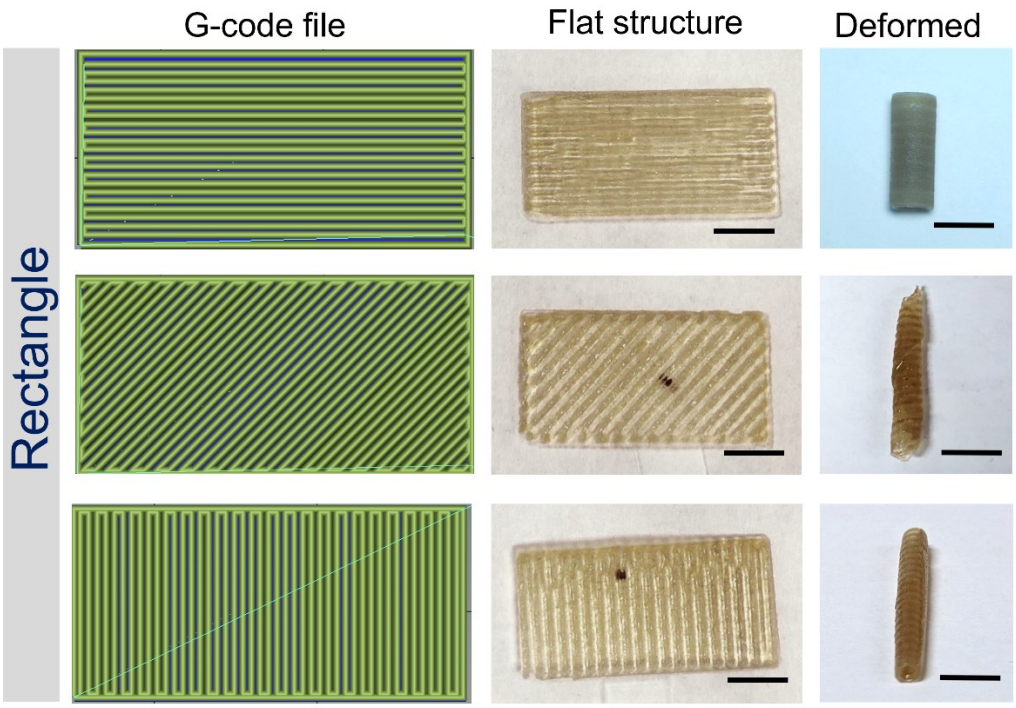


**Fig. S12:** G-codes of different tubular geometries and subsequent experimental validation of the effect of stripe angle (0º, 45º, and 90º) on corresponding deformations. The scale bar is 4 mm.

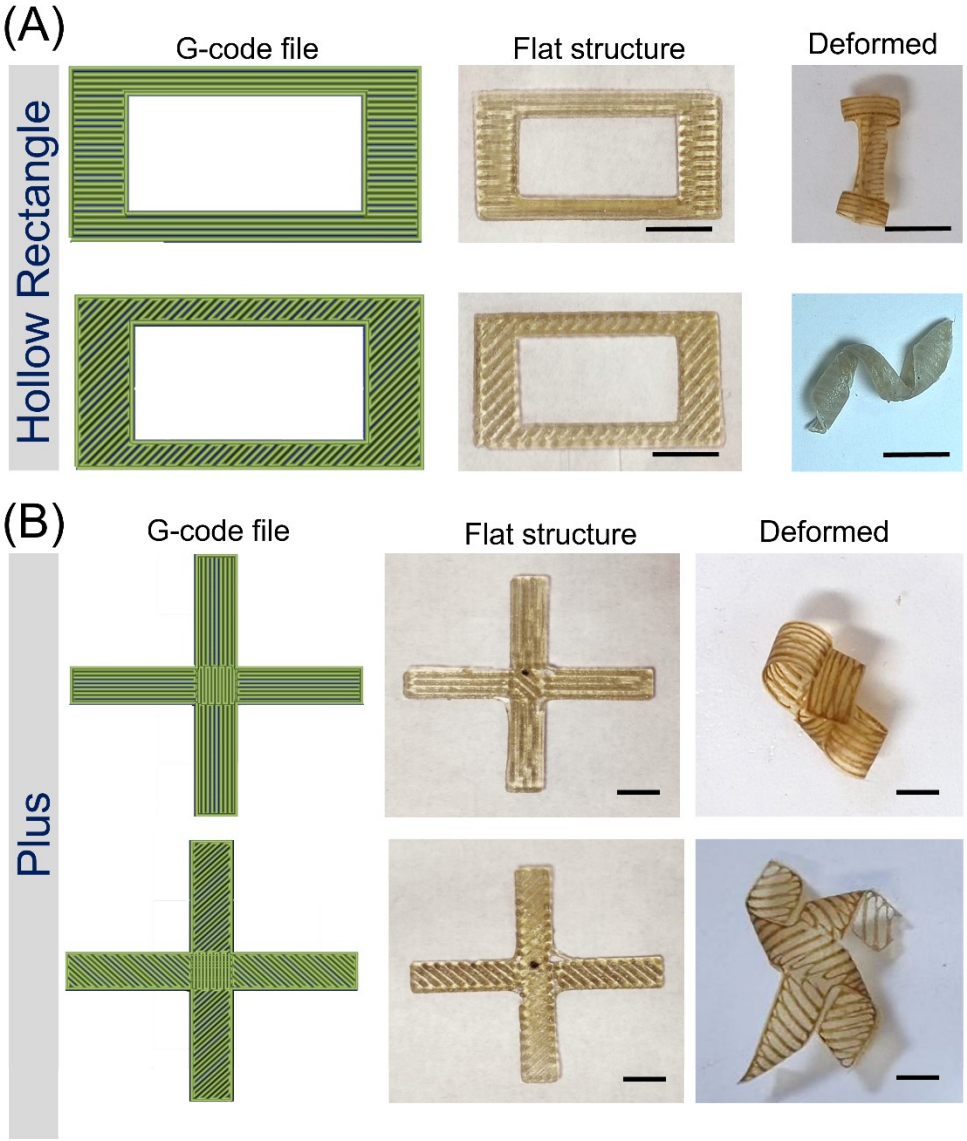


**Fig. S13:** Experimental validation of (A) hollow rectangle and (B) plus-shaped geometries. The G-codes were created based on predictive computational designs and the subsequent effect of stripe angles (0º, 45º, and 90º) on shaped deformation. Scale bars in (A) and (B) are 10 mm and 7.5 mm, respectively.

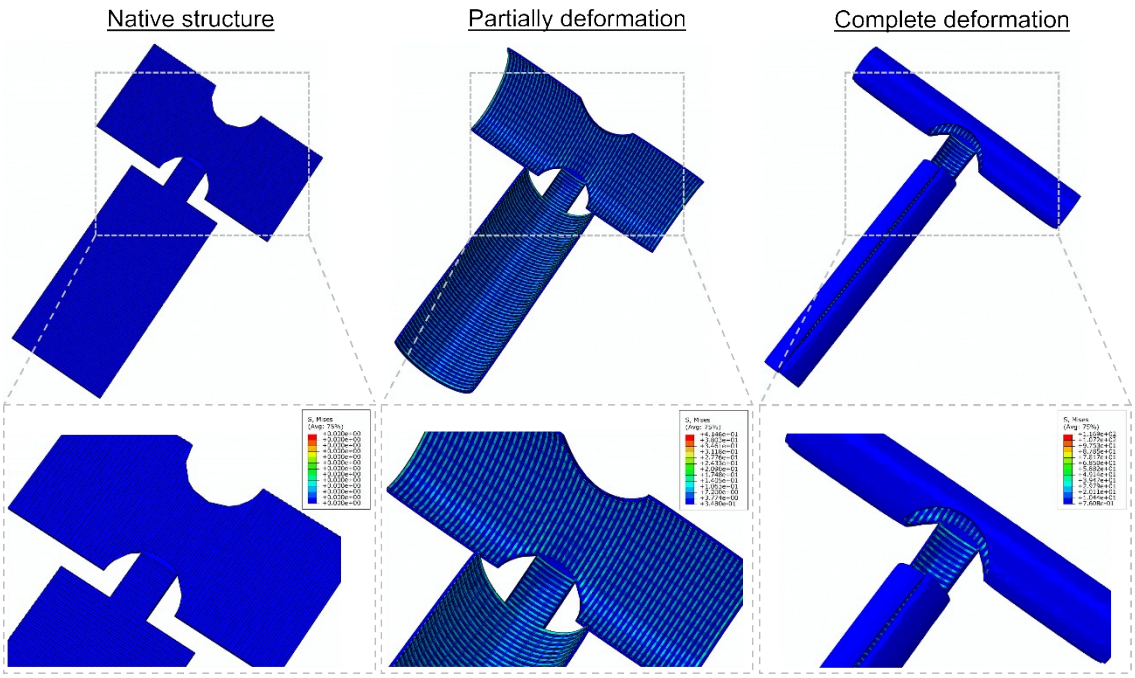


**Fig. S14:** 3D representation of FEA simulations of T-shaped deformations.